HHS Public Access

Author manuscript

Matrix Biol. Author manuscript; available in PMC 2015 July 02.

Published in final edited form as:

Matrix Biol. 2011 June ; 30(0): 318–329. doi:10.1016/j.matbio.2011.05.003.

Caveolin-1 modulates TGF-β1 signaling in cardiac remodeling

Shelley K. Miyasato[a], **Jorik Loeffler**[a], **Ralph Shohet**[b], **Jianhua Zhang**[c], **Merry Lindsey**[c], and **Claude Jourdan Le Saux**[a,d]

[a]University of Hawaii, John A. Burns School of Medicine, Honolulu, Hawaii, USA, Dept. of Cell and Molecular Biology

[b]Dept. of Medicine, and UT Health Science Center San Antonio, Texas, USA.

[c]Dept. of Medicine Geriatric, San Antonio, Texas, USA.

[d]Dept. of Cardiology Division, San Antonio, Texas, USA.

Abstract

The cardiac response to myocardial injury includes fibrotic and hypertrophic processes and a key mediator in this response is transforming growth factor-β1 (TGF-β1). Caveolin-1 (cav1), the main structural protein of caveolae, is an inhibitor of the TGF-β1 signaling pathway. To examine the role of cav1 in cardiac repair, cav1 deficient (*Cav1*$^{-/-}$) and wild type (WT) mice were subjected to cryoinjury of the left ventricle (LV). At baseline the two groups exhibited no inflammation, similar collagen content, and similar cardiac function. After injury, *Cav1*$^{-/-}$ animals displayed enhanced TGF-β1 signaling, as reflected by a 3-fold increase in the activation of the Smad2-dependent pathway and more widespread collagen deposition in the heart. Qualitative and quantitative analysis indicated that collagen deposition peaked in the WT LV 14 days after injury, accompanied by increased mRNA abundance for *procol1a2* (2-fold) and *procol3a1* (3-fold). Collagen deposition was further enhanced in *Cav1*$^{-/-}$ mice, which was accompanied by reduced expression of matrix metalloproteinases MMP −8 (3-fold) and −13 mRNA (2-fold). The levels of expression of inflammatory markers of acute phase were similar between the strains However, macrophage clearance in the damaged region was delayed in *Cav1*$^{-/-}$ mice. We observed a 4-fold decrease in collagen deposition in *Cav1*$^{-/-}$ mice injected with a cav1 scaffolding domain peptide (CSD) and a 2-fold decrease in WT mice treated with the CSD. We conclude that cav1 has a direct role in reducing TGF-β1 signaling and as such might be an appropriate target for therapies to influence cardiac remodeling.

Corresponding Author Claude Jourdan Le Saux, Ph.D. University of Texas Health Science Center at San Antonio Dept of Medicine-Cardiology MC-7872 7703 Floyd Curl Drive San Antonio, Tx 78229-3900 lesaux@uthscsa.edu Tel: 210 567 4613 Fax: 210 567 6960.

skmiyasa@hawaii.edu (SK. Miyasato); shohet@hawaii.edu (R. Shohet); ZHANGJ0@uthscsa.edu (Z. Jiuang); lindseym@uthscsa.edu (M. Lindsey)

Keywords

Caveolin-1; TGF-β1 signaling; cardiac remodeling; mouse model; cryoinjury

1. Introduction

Immediately after myocardial injury, cardiomyocyte necrosis induces an immune response mediated by the cytokines interleukin (IL)-1β, IL-6, tumor necrosis factor-α (TNF-α), and transforming growth factor-β1 (TGF-β1). Subsequently, monocytes infiltrate the area, clearing out debris, and releasing growth factors that stimulate fibroblasts. Activated fibroblasts synthesize extracellular matrix (ECM) that forms scar tissue. As the region of necrosis matures, the remaining myofibroblasts undergo apoptosis, leaving behind a fibrous scar that can impair mechanical properties of the ventricle. With its pleiotropic effects, TGF-β1 is a key mediator of these processes (Bujak & Frangogiannis 2007). TGF-β1 is involved in cell proliferation, apoptosis, migration, immune regulation, and ECM synthesis and degradation. TGF-β1 attracts monocytes to the necrotic tissue during the inflammation phase, but also later promotes the deactivation of monocytes. It also activates ECM production and maintenance during the maturation and repair phases. Therefore, TGF-β1 regulation is important in injured myocardium.

Caveolin-1 (cav1) is a negative regulator of TGF-β1 signaling (Galdo et al 2008, Le Saux et al 2008, Lee et al 2007, Razani et al 2001). As the main structural protein of caveolae, which form omega-shaped invaginations of the plasma membrane, cav1 is expressed by many cell types including fibroblasts, endothelial cells and smooth muscle cells. These membrane compartments concentrate signaling molecules, including the TGF-β receptors, TbRI and TbRII. TGF-β1 signaling pathways are mediated by the receptor-associated TGF-β1 receptor complex, which leads to the activation of Smad proteins and mitogen-activated protein kinases (MAPKs) that ultimately regulate the transcription of target genes. TGF-β1 signaling is tightly regulated at multiple levels, including association with various extracellular matrix components and transmembrane proteins, notably cav1 (Duvernelle et al 2003, Munger et al 1997). Cav1 regulates TGF–β1 signaling through receptor gene expression and receptor turnover (Zhang et al 2005). Moreover, the scaffolding domain of cav1 interacts directly with TbRI to prevent kinase activity, effectively blocking the TGF-β/SMAD pathway (Tourkina et al 2008, Wang et al 2006).

At younger ages (up to 8 weeks), cav1 deficiency in mice does not lead to impaired cardiac function (Chow et al). In aged animals, however, changes in function and in morphology of the heart have been reported (Augustus et al 2008, Cohen et al 2003, Murata et al 2007, Zhao et al 2002). Decreased systolic function associated with left and right ventricular hypertrophy has been reported in 6-month and older animals along with depressed cardiac contractility. Increased vascular permeability is also observed in these mice. The function of cav1 in response to cardiac injury is not well defined. Cav1 has been associated with effects ranging from cardiac protection to cardiac contractile dysfunction (Patel et al 2007, Young et al 2001). In this study, we identified a novel role for cav1 in regulating cardiac TGF-β1 signaling after myocardial injury. We hypothesized that *Cav1*$^{-/-}$ mice would enhance

TGFβ1 signaling due to reduced cav1-mediated inhibition, with subsequent effects on cardiac remodeling. Cardiac remodeling was studied in a left ventricular cryoablation model by histological quantitation of fibrosis, and biochemical determination of collagen and metalloproteinase gene expression. Signaling was also studied in isolated cardiac fibroblasts from WT and *Cav1*$^{-/-}$ mice.

2. Results

2.1 Downregulation of caveolin-1 after cryoablation

To evaluate the role of cav1 in cardiac remodeling, we measured temporal profiles of cav1 expression and TGF-β1 signaling after cryoablation in WT animals. We then compared remodeling parameters in *Cav1*$^{-/-}$ mice to those obtained in WT mice.

We investigated the expression of cav1 by semi-quantitative real-time PCR and western blot in whole hearts. The amount of *cav1* mRNA fell by 2-fold in cryoinjured mice compared to sham-operated animals after 3 days ($p<0.001$, Figure 1A). Western blot assays confirmed a decrease in cav1 protein (1.5-fold reduction, $p<0.05$) (Figure 1B). At 14 days post injury, the levels of cav1 (mRNA and protein) returned to those seen in sham-operated mice. To identify the cell type responsible for reduced expression of cav1, we used immunohistochemistry and showed that Cav1 expression by endothelial cells was reduced at 3 days after cryoinjury and returned to normal (Figure 1C) by 14 days. Three days after cryoinjury, as expected, we observed an increase of DDR2 by immunofluoresent detection in activated fibroblasts in the injured zone that was interestingly not associated with an increase in cav1 expression (data not shown).

2.2 General and Histological evaluation of the Cav1$^{-/-}$ mice heart compared to WT after cryoinjury

The increase in heart/body weight ratio was larger in the *Cav1*$^{-/-}$ mice 3 days after cryoinjury (0.86 ± 0.23 mg/g in C*av1*$^{-/-}$ mice vs. 0.6 ± 0.1 mg/g in WT, $n = 10$, $p<0.001$) (Figure 2A). To evaluate one possible cause of the heart weight difference, we explored whether this increase was the result of edema. Significant amounts of Evans Blue dye were found in hearts of injured *Cav1*$^{-/-}$ mice and not in the injured WT mice, which is consistent with increased permeability of the endothelial barrier (Figure 2B). Total collagen content was not different 3 days after injury in *Cav1*$^{-/-}$ and WT mice (Figure 2C) suggesting that the increase in weight in *Cav1*$^{-/-}$ mice was not due to increased fibrosis at this early time-point after injury.

2.3 Increased interstitial collagen deposition in the injured Cav1$^{-/-}$ but not perivascular collagen deposition as observed in injured WT

The cryoinjury method selected for this study produced an injury of consistent shape and size among the animals, as expected (O'Quinn et al 2011, van den Bos et al 2005. Three days after LV cryoinjury, HE staining showed a discrete border between necrotic tissue and viable myocardium in both strains (Figure 3A). In sham-operated mice, the collagen deposition in the myocardium and around the vessels in the heart did not differ between *Cav1*$^{-/-}$ and WT mice. Trichrome staining revealed that 14 days after cryoinjury, collagen

deposition in the injured heart was different between *Cav1*$^{-/-}$ and WT animals (Figure 3B). *Cav1*$^{-/-}$ mice showed the development of fibrous deposition extending from the injured zone into the myocardium. By contrast, WT mice showed primarily a perivascular fibrosis in the injured region of the heart. After 1 month, *Cav1*$^{-/-}$ mice showed persistent interstitial collagen deposition while the WT mice showed regression of fibrosis. Quantitation of picrosirius red staining confirmed the enhanced and differential deposition of collagen in *Cav1*$^{-/-}$ mice compared to WT animals (Figure 4).

Procollagen1a2 and *procol3a1* gene expression was examined by semi-quantitative real-time PCR in the hearts of *Cav1*$^{-/-}$ and WT mice. *Procol1a2* and *procol3a1* mRNA abundance were similar in sham-operated animals from the 2 groups. The profiles of *procol1a2* and *procol3a1* expression were also similar in direction but not in magnitude in *Cav1*$^{-/-}$ and WT mice after cryoinjury. We measured a peak of mRNA abundance in the 14-day samples from both groups but more pronounced in injured hearts of *Cav1*$^{-/-}$ mice and a return to baseline in 30-day samples (Figure 3C). We also measured by western blot a 2-fold increase of HSP47, a surrogate marker for collagen deposition, in injured hearts of *Cav1*$^{-/-}$ (3 and 14 days post injury) and WT mice (14 days post injury) compared to their sham-operated counterparts. At 3 days post injury, the level of expression of HSP47 was similar between the WT and Cav1$^{-/-}$.

To evaluate the catabolism of collagen, we considered the expression of two principal collagenases (*MMP-8*, and *−13*) (Figure 5A). Three days post injury, *MMP-8* was more abundant only in WT animals and the abundance of *MMP-13* mRNA was less pronounced in *Cav1*$^{-/-}$ hearts compared to WT. In addition, a substantial increase in total MMP activity was measured in WT heart 3-day after injury but not in *Cav1*$^{-/-}$ mice (Figure 5B), indicating that the accumulation of collagen observed in *Cav1*$^{-/-}$ mice 1 month following the injury is, in part, the result of reduced degradation. We also evaluated mRNA abundance of *MMP-2* and *MMP-9*. *MMP-2* mRNA was increased after cryoinjury in both strains. However the increase was more pronounced at 14 days following cryoinjury in the *Cav1*$^{-/-}$ mice. We observed an increase in *MMP-9* mRNA in *Cav1*$^{-/-}$ mice only 3 days post injury (Figure 5A).

2.4 Acute phase inflammatory markers expression after cryoablation

In the absence of injury, *Cav1*$^{-/-}$ hearts did not show signs of spontaneous inflammation (Table 1, sham-operated animals). At baseline, no difference was observed in cell counts (neutrophils and macrophages) or the levels of mRNA expression of the tested cytokines (IL-1β, IL-6, TNF-α, and TGF-β). After cryoinjury, infiltration of the injured zone with neutrophils and macrophages was observed in both WT and *Cav1*$^{-/-}$ mice (Table 1). Compared to WT, the density and clearance of neutrophils was not different in *Cav1*$^{-/-}$ mice. Interestingly, the macrophage density peaked at 3 days after injury for both strains but the clearance was altered in *Cav1*$^{-/-}$ mice, consistent with the peak of expression of *MMP-9* mRNA. Return to baseline was observed by 14 days post injury in the null mice, in contrast to WT, where return to baseline was seen only at 30 days after injury. These data suggest that cav1 deficiency alters the time course of resolution of the inflammation in relation to macrophage clearance.

2.5 Activation of TGF–β1 signaling pathways after cryoablation

We also demonstrated by western blot that these injured hearts had increased pSmad2 expression after 3 days, inversely mirroring cav1 expression in WT animals, while total Smad2 levels remained the same. This increased ratio of pSmad2 to Smad2 indicates an activation of the Smad2/3 pathway (Figure 6A). Moreover, this increase was more pronounced in the *Cav1*$^{-/-}$ cryoinjured mice compared to WT (Figure 6A), supporting an inverse association between the level of cav1 and activation of the canonical TGF-β1 signaling pathway. Cav1 is also known to regulate TGF-β-dependent MAPK signaling pathways. In sham-operated *Cav1*$^{-/-}$ mice, the ratio between pERK1:ERK1 was higher compared to WT, at all time points (Figure 6B). After cryoinjury, we did not observe increased activation of ERK1 in either WT or *Cav1*$^{-/-}$ mice. Changes in signaling returned to baseline level by 30 days after injury in both groups, while cav1 expression also returned to baseline.

2.6 Cav1$^{-/-}$ cardiac fibroblasts are more responsive to TGF-β1 stimulation

To determine whether caveolin-1 participates in the regulation of TGF-β1 signaling in cardiac fibroblasts, we studied *in vitro* the response of isolated cardiac fibroblasts to TGF-β1 stimulation. We measured the level of expression of luciferase gene reporter expression under the control of the Smad response element and found that the activity of transfected reporter constructs was more pronounced in the *Cav1* $^{-/-}$ cardiac fibroblasts (Figure 7). These data confirmed in cardiac fibroblasts as previously described in other systems, that TGF-β1 signaling is controlled by cav1 and as the result, increased TGF-β–Smad-dependent gene expression is more pronounced in *Cav1*$^{-/-}$ cells.

2.7 Caveolin-1 scaffolding domain treatment protects against cryoablation-induced myocardial fibrosis

To confirm the protective role of cav1 in the development and progression of myocardial fibrosis, we tested whether administration of the CSD to WT and *Cav1*$^{-/-}$ mice could prevent the development of fibrosis following cryoinjury. As previously shown, the peak of fibrosis was observed at 14 days post injury and we therefore selected this time point to collect hearts. The mice treated with cav1 scaffolding domain, showed reduced collagen deposition compared to animals that were given a scrambled peptide, as measured by picrosirius red stain (Figure 8A, B). More impressively, the protective effect of the cav1 peptide treatment was clearly evident in *Cav1*$^{-/-}$ mice. We observed a reduction in interstitial fibrosis and in the development of perivascular fibrosis in CSD-treated *Cav1*$^{-/-}$ mice. In cryoinjured *Cav1*$^{-/-}$ heart samples, we measured a reduced expression of *procol1a2* mRNA after cav1 scaffolding domain peptide (CSD) treatment that was not observed with scrambled peptide negative control treatment (Figure 8C). In contrast, *procol3a1* mRNA expression was not reduced after the CSD treatment (data not shown). This finding indicates that the increase in expression of *procol1a2* after cryoinjury is in part controlled by cav1. In addition, cryoinjured mice treated with the cav1 scaffolding domain had reduced activation of the canonical TGF-β1 signaling pathway (Smad2 dependent) and non-canonical pathways (ERK1) in both strains (Figure 9). These data show that the activation of these TGF-β1 dependent pathways is also cav1-dependent.

3. Discussion

Cav1 gene and protein expression are transiently down-regulated after cryoablation, concomitant with activation of the downstream Smad signaling pathway in cardiac fibroblasts. Furthermore, in the absence of cav1 expression, the alterations in remodeling that we see are consistent with enhancement of TGF-β1 signaling activity after myocardial injury. We also demonstrate that restoration of cav1 inhibition of TGF-β1 signaling with a scaffolding domain peptide reduces collagen deposition. Interestingly, a recent study indicates that cav1 participates in cardiac protection, and is expressed by myocytes (Kozera et al 2009, Patel et al 2007, Volonte et al 2008). There is little information regarding how cav1 regulates myocardial responses in animal injury models or human pathologies. However there is some indirect evidence that cav1 plays a role in human cardiovascular pathologies. Telomerase-independent cell senescence is regulated by cav1 in endothelial cells from artherosclerotic patients and contributes to the pathogenesis of this cardiovascular disease (Farhat et al 2008, Voghel et al 2007). Another indirect evidence of the potential relevance of cav1 to human myocardial injury comes from the interaction between connexin 43 and cav1. Connexin 43 expression varies in cardiac pathologies and its function has been shown to be regulated by cav1 (Barth et al 2005, Langlois et al 2008, Schubert et al 2002).

Remodeling following cardiac injury is one cause of LV dysfunction. We specifically selected the cryoinjury model as our experimental model of myocardial wound healing to reduce the inter-animal variability of the damaged regions without compromising the inflammatory reaction. Lesions formed after cryoinjury have been reported to heal without disturbing the surrounding myocardial anatomy or causing arrhythmias (Jensen et al 1987, O'Quinn et al 2011, van den Bos et al 2005). We observed a different distribution and magnitude of collagen deposition in the cav1$^{-/-}$ 14 days after injury. Both gene expression and biochemical detection indicate a more pronounced collagen deposition in *Cav1*$^{-/-}$ mice. The WT animals exhibited collagen deposition around the vessels, while *Cav1*$^{-/-}$ mice had increased interstitial deposition. Cav1 is expressed by the endothelial cells and our qualitative evaluation suggested that the downregulation of cav1 was mainly observed in these cells rather than the fibroblasts. Interestingly and reinforcing the importance of these data, re-expression of cav1 in endothelial cells alone rescues elements of the cav1-deficient mouse phenotype, particularly in the heart (Murata et al 2007). It may not be surprising then that following the initial decreased cav1 expression after injury in the endothelial cells, the return to baseline cav1 expression is associated with regression of collagen expression and recovery to almost normal histology 30 days after injury.

Excessive collagen deposition in the heart contributes to heart failure, and for this reason, controlling collagen homeostasis might a suitable target for therapeutic intervention. Collagen deposition is the result of a balance between the expression of collagen genes and its degradation by MMPs. It has been shown that high myocardial collagenase expression (MMP1 and MMP8 particularly), without compensatory changes in collagen or TIMP expression, is associated with a poor outcome in heart failure patients (Martos et al 2009, Radauceanu et al 2008, Vanhoutte & Heymans 2009). In the LV, fibrillar collagen I and III are the major components of the extracellular matrix and are synthesized by cardiac fibroblasts. As we measured increased expression and deposition of collagen proteins after

cryoablation, we further investigated the regulation of *procol1a2* and *procol3a1* gene expression and their MMP counterparts (*MMP-8* and *−13*). The levels of *procol1a2* and *procol3a1* expression peaked at 14 days post injury in both strains but the increased was more pronounced in the *Cav1*$^{-/-}$ mice. Expression of collagen genes and the surrogate marker of collagen deposition, HSP47, could not solely account for the difference in quantity and distribution of collagen deposition. We found evidence that in the absence of cav1, reduced expression of collagenases and reduced total MMP activity may also contribute to collagen accumulation.

We also reported the activation of MMP-2 and −9 expression following cryoinjury. Interestingly but not entirely surprisingly, the expression of these MMPs was more pronounced in *Cav1*$^{-/-}$ mice. Indeed cav1 has been shown to regulate the expression of MMP-2 (Chow et al 2007). Without injury, Chow et al. reported that MMP-2 activity was enhanced in *Cav1*$^{-/-}$ heart compared to WT, indicating that cav1 participates in the regulation of MMP-2 activity. Our data suggested that cav1 may also play a role in the regulation of MMP2 expression after heart injury. In a mammary tumorigenesis and lung metastasis mouse model, the overexpression of cav1 results in a marked reduction of MMP-2 and MMP-9 secretion (Williams et al 2004). Our data support these studies and clearly indicate that cav1 regulated the expression and activation of MMP-2 and −9.

Each of these proteins (collagen and collagenase) is regulated by TGF-β1. Therefore controlling TGF-β1 expression and signaling may provide an approach to reducing the hemodynamically unfavorable aspects of pathological remodeling. The canonical TGF-β1 signaling pathway involves the activation by phosphorylation of several transduction proteins that belong to the Smad family, of which 8 members have been identified. To better understand the importance of the various components of the TGF-β1 signaling cascade in heart remodeling, mouse models have been intensively studied. Deletion or overexpression of each Smad protein has a different primary effect. For instance, absence of Smad3 was shown to impact primarily fibrotic remodeling in cardiac injury while disruption of Smad4 resulted in cardiac hypertrophy, and overexpression of I-Smad7 impacted cardiac fibroblast activation and function (Bujak et al 2007, Hao et al 1999, Wang et al 2002, Wang et al 2007, Wang et al 2005). Various studies have also highlighted the negative regulatory role of cav1 in the activation of Smad2/3 in a variety of tissues and pathologies (Del Galdo et al 2008, Galdo et al 2008, Le Saux et al 2008, Wang et al 2006, Young et al 2001, Zhao et al 2002).

Cav1 deficiency does not appear to be associated with major changes in the inflammatory response, except for altering the clearance kinetics of macrophages. However this difference may play a more important role than expected, as this faster clearance could lead to impaired wound healing and contribute to some of the remodeling observed in *Cav1*$^{-/-}$ mice. Depletion of infiltrative macrophages has been shown to impair wound healing and increase LV remodeling using the same cryoinjury mouse model (van Amerongen et al 2007). Our findings suggest that cav1 could regulate not only the fibrotic but also the inflammatory phases that follow cardiac injury.

In our study, absence of cav1 expression leads to increased fibrosis *in vivo* and enhanced TGF-β1 signaling in cardiac fibroblasts *in vitro*. Cav1 has been shown to block TGF-β1

signaling pathway by either directly interacting with TGF-β receptor I and preventing the downstream phosphorylation of Smad2/3 or by promoting TGF–β receptors internalization in cav1-positive vesicles leading to TGF-β receptors degradation (Chen 2009, Lee et al 2007, Razani et al 2001). The putative mechanism by which cav1 reduces TGF-β1 activity involves scaffolding of the TGF-β receptor and consequent inactivation of the signaling pathway.

Previous studies have shown that administration of cav1 scaffolding protein inhibits bleomycin-induced inflammation and fibrosis, and inhibits synthesis of NO, and reduces inflammation following acetylcholine-induced vasodilation and NO production (Bucci et al 2000). Cav1 regulates collagen synthesis via a complex mechanism involving the Smad-dependent and ERK-dependent signaling pathways. We demonstrated that both pathways were suppressed after CSD peptide infusion in association with reduced collagen expression. Furthermore, treatment of *Cav1*$^{-/-}$ with CSD not only prevented the excess collagen expression, but also restored the deposition to the WT perivascular pattern. These data suggest that cav1 not only regulates the expression and deposition of collagen, but may also be cell specific. Our work reinforces the notion that there is a time and cell specific regulatory mechanism for TGF-β1 signaling inhibitors and there is a great need to elucidate their relative role in order to design efficient therapeutic strategies.

In our study, we assessed the time course of cav1 expression and its effect on the activation of TGF–β1 signaling as it has been reported that anti-TGF-β treatments need to be timed carefully. In the WT mice, we measured a transient down-regulation of cav1 during the inflammatory phase while in the proliferative and maturation phase the expression of cav1 returned to the level in sham-treated animals. In the WT mice, it appears that the pattern of cav1 expression and its consequence on TGF-β1 signaling regulation is favorable to promote healing and repair. By contrast, in the *Cav1*$^{-/-}$ mice, the lack of cav1 is associated with excessive collagen deposition. This suggests that failure to re-express cav1 during the maturation phase could be associated with heart failure. The current study suggests a critical role for cav1-mediated regulation of TGF-β1 activity during cardiac injury and repair.

4. Experimental Procedures

4.1 Mouse Strains

Wild type C57BL/6J (WT) and Cav$^{tm1Mls/J}$ (*Cav1*$^{-/-}$) mice were purchased from The Jackson Laboratory (Bar Harbor, Maine). The *Cav1*$^{-/-}$ mice were backcrossed with C57BL/6J mice for at least 6 generations to obtain a homogeneous genetic background. Animal experiments were conducted in compliance with a protocol approved by the Institutional Animal Care and Use Committee of the University of Hawaii.

4.2 Cryoablation and caveolin-1 scaffolding domain treatment

Male mice, 8 – 10 weeks of age, weighing at least 20 g were included in this study (n=5 to12 per group). For cryoablation, mice were anesthetized by intraperitoneal injection of ketamine/xylazine (King Pharmaceuticals Inc. Bristol, TN and Science Lab, Houston, TX) at 50/10 mg/kg, intubated, and ventilated with an Inspira Ventilator (Harvard Apparatus,

Holliston, MA). The pericardial thoracic cavity was entered between the third and fourth intercostal space and ribs were gently retracted. A 4 mm probe previously cooled in liquid nitrogen was applied to the left ventricular apex for 7-8 sec to obtain a well-defined area of cryoablation. The pleural cavity was closed with 6.0 silk. Mice were extubated and placed in a warmed, oxygen enriched environment to recover before return to a normal cage environment. Sham-operated animals were prepared identically except for application of the cooled probe.

Ten additional cryoinjured WT mice per subgroups were treated with the cav1 scaffolding domain (CSD). In the first subgroup labeled 14d the mice were treated for 14 days after cryoinjury with the CSD or scrambled peptide. In the second subgroup labeled 7d, the mice were treated for 7 days starting 7 days after cryoinjury. We used the CSD and its scrambled peptide as described by Tourkina et al. (Tourkina et al 2008) as follows: The CSD peptide (amino acids 82–101 of caveolin-1; DGIWKASFTTFTVTKYWFYR) and a scrambled control peptide (WGIDKAFFTTSTVTYKWFRY) were synthesized fused to the COOH terminus of the antennapedia internalization sequence (RQIKIWFQNRRMKWKK) (Invitrogen). Before each experiment, lyophilized peptides were dissolved at a 0.5 mM final concentration in 10% DMSO as described by Bernatchez et al. (Bernatchez et al 2005) and delivered by Alzet osmotic minipumps that deliver 0.5 μl per hour for one week (Model #1007D, Durect Corporation, Cupertino, CA). Whole hearts were harvested 14 days after cryoablation for histological evaluation and RNA and protein extraction.

4.3 Histology and Immunohistochemistry

Heart tissues were fixed in 4% paraformaldehyde and embedded in paraffin. Sections were cut 5-μm thick and stained with Masson's Trichrome or Picrosirius Red. All slides were processed as a batch under identical conditions. For immunohistochemistry, paraffin embedded tissue sections were stained with 1:100 anti-cav1 (Cell Signaling) following antigen retrieval with 10 mM sodium citrate pH 6. Staining was conducted with Vectastain ABC Kit for peroxidase systems (Vector, Burlingame, CA) and the DAB chromogen with hematoxylin counterstain according to manufacturer's instructions. For immunofluoresence, paraffin-embedded tissue sections were stained with 1:100 anti-DDR2 (Santa Cruz, Santa Cruz, CA) followed with Texas Red labeled secondary antibody (Jackson ImmunoResearch Laboratories, West Grove, PA).

4.4 Cardiac permeability and edema

Cardiac permeability was evaluated using Evans Blue injection. After i.p. anesthesia with ketamine (50 mg/kg) and xylazine (10 mg/kg), Evans Blue (20 mg/kg) was injected into the tail vein at a concentration of 5 mg/ml. Mice were sacrificed 24 hr after injection and hearts were perfused with 5 ml of PBS through the left ventricle. Measurement of Evans Blue that diffused into the cardiac tissue was performed as previously described (Wang le et al 2002). Briefly, whole hearts were homogenized in PBS and 15 volumes of formamide and incubated at 60°C for 12 hr. After centrifugation at 5,000xg for 30 min, the supernatant was collected and absorbance was measured at 620 nm and 740 nm. Evans Blue content (mg EB/g heart) was determined after adjusting values at 620 nm for the presence of heme

pigments thusly: corrected absorbance at 620 nm = A620 – (1.426 × A740 + 0.030). Results were calculating using a standard curve of Evans Blue in formamide/PBS.

4.5 Gene and protein expression

Total RNA was extracted from myocardial samples using the RNeasy™ kit (Qiagen Inc., Valencia, VA). RNA samples were treated with 0.05 U/ml of DNAse I (Qiagen) at 20°C for 15 min. Total RNA (1 μg) was converted into first-strand cDNA using random hexamers (SuperScript III First-Strand Synthesis System for RT-PCR™, Invitrogen Life Technologies, Carlsbad, CA). The relative abundance of mRNA for *cav1*, alpha 2 chain of type I procollagen (*procol1a2)*, alpha1 chain of type III procollagen (*procol3a1*), metalloproteinase-2 (*MMP-2*), *MMP-8*, *MMP-9*, *MMP-13*, interleukin-1β (IL-1β), IL-6, TGF-β, and tumor necrosis factor-alpha (TNF-α) mRNA was detected by semi-quantitative RT-PCR (qPCR) using commercially available TaqMan probes (Applied Biosystems, Foster City, CA). Results were analyzed by ΔΔCt method with GAPDH or β-actin as the endogenous control.

Total protein was extracted by homogenizing frozen heart tissues on ice in lysis buffer (10 mM Tris pH 7.5, 50 mM NaCl, 50 mM NaF, 60 mM octylglucoside, 1 mM sodium vanadate, 1mM β-glyceophosphate, 2.5 mM sodium pyrophosphate, 2 μM EDTA, 1x protease inhibitor cocktail (Roche, Indianapolis, IN), 1% Triton X-100). Homogenates were centrifuged at 16,000xg and the protein concentration in the supernatant was determined by the Bradford assay (Bio-Rad, Hercules, CA). Total protein (15 μg) was combined with reducing Laemmli buffer, heated at 95°C for 10 min, cooled on ice, and subjected to electrophoresis through a 10% polyacrylamide gel. Protein was transferred to PVDF membrane and blotted with primary antibodies including anti-cav1 (Fitzgerald, Concord, MA), anti-Smad2, anti-phospho-Smad2, anti-ERK1/2, and anti-phospho-ERK1/2 (Cell Signaling, Danvers, MA). Appropriate peroxidase-linked secondary antibodies were detected using ECL Plus (Amersham, Piscataway, NJ). For densitometry, digital images of autoradiographic film were captured using Gel Logic 200 and Kodak MI software (Kodak Scientific Imaging Systems, Rochester, NY). The net intensity of the target bands on an undersaturated exposure was normalized to GAPDH to obtain a relative level of proteins of interest.

For evaluation of collagen content, we used the Sircol Collagen Assay kit (Biodye Science, Westbury, NY) according to the manufacturer's instructions. Briefly, 50 mg of whole heart tissue was homogenized in 500 μl of extraction buffer™ and incubated for 12 hr at 4°C with stirring. Tissue homogenates were spun at 15,000 x g for 60 min at 4°C. Aliquots of heart homogenate were then assayed for total collagen levels by comparison with a standard curve of collagen obtained by optical density at 540 nm with a SpectraMAX 340 (Molecular Devices, Toronto, Canada).

4.6 Metalloproteinase Activity

Heart samples were homogenized in 1 ml of lysis buffer (Cell Lytic MT from sigma + complete mini EDTA-free from Roche), then sonicated with 30 pulses. The samples were spun at 15,000xg for 15 min and aliquots were stored at −80°C. The OmniMMP™

fluorogenic substrate (P-126, Biomol International, Plymouth Meeting, PA) was used to analyze total metalloproteinase activity in heart homogenates. Samples (25 μl) were added to 96-well plates and warmed to 37°C. Substrate was added to each well, and the plate was read immediately (excitation: 328 nm; emission: 393 nm) and then again at 1.5, 3, 6, 12, 30, 60, 120, and 240 min with a Synergy 4 (BioTek Instruments, Inc., Winooski, VT). The increase in fluorescence was plotted against time, and the slope of the line, which indicates metalloproteinase activity, was determined using GraphPad Prism for Macintosh version 4.0c (GraphPad Software, Inc., San Diego, CA). Metalloproteinase activity was normalized to total protein for each well.

4.7 Evaluation of inflammatory cell infiltration

Macrophage and neutrophil infiltration were detected in 5 μm thick paraffin embedded tissue sections. Antigen retrieval was performed with citrate buffer pH 6.2 (10mM citric acid, 2mM EDTA. 0.05% tween-20) at 95°C for 20 min, followed by quenching of endogenous peroxidase with 0.3% hydrogen peroxide in methanol. The tissue was then stained with 1:500 rat anti-mouse Mac2 (Cedarlane, Burlington, Ontario, Canada) or 1:1000 rat anti-mouse neutrophils (AbD Serotec, Raleigh, NC) using the Vectastain Elite ABC Kit (rat IgG) for peroxidase systems and developed with diaminobenzidine+nickel (Vector, Burlingame, CA) according to manufacturer's instructions. Macrophages (600× magnification) and neutrophils (400× magnification) were counted using a 10mm × 10mm eyepiece grid. Six grids for macrophages and 4 grids for neutrophils were counted at the apex of the heart in the area of cyroablation.

4.8 Isolation and stimulation of murine cardiac fibroblasts

To isolate cardiac fibroblasts, minced WT and *Cav1*$^{-/-}$ hearts were digested for 45 min at 37°C in complete medium (DMEM, 10% FBS, 100 units/ml penicillin G sodium and streptomycin, 0.25 μg/ml amphotericin B) with 0.5 mg/ml Liberase CI and 30 mg/ml DNAse I. Cells were passed through a 40 μm nylon cell strainer and cultured in complete medium. Cardiac fibroblasts were used at confluence between passage 3 and 5. Transient transfections of pGL3-ti (SBE)4 (generously provided by Dr. Aristidis Moustakas, Ludwig Insitute for Cancer Research, Uppsala, Sweden) and a pRL-SV40 control plasmid were performed using the GeneJammer transfection reagent (Stratagene, La Jolla, CA) as described by the manufacturer. The pGL3-ti (SBE)4 plasmid contains the luciferase reporter gene under the regulation of the smad response element. Cells were treated with TGF-β1 (2ng/ml) at the end of the transfection procedure for 24 hr and luciferase activity was determined with the Dual Luciferase Reporter Assay System (Promega, Madison, WI) using a Model TD-20/20 Luminometer (Turner Designs, Sunnyvale, CA).

4.9 Statistical Analysis

Results are expressed as mean ± standard deviation (SD). ANOVA followed by a Tukey post-test was used to compare between multiple groups. A p-value <0.05 was considered significant. Data entry, management and statistical analysis were performed using Prism software (GraphPad Software, San Diego, CA).

Acknowledgements

We would like to thank Dr. Mark Entman and his laboratory for valuable scientific discussion and advice and Drs. Parks and Gill for the assay on total MMP activity.

This work was supported by NIH-NCRR RR016453 (Drs. Shohet and Jourdan Le Saux), NHLBI HL073449 (Dr. Shohet), NHLBI HL75360 (Dr. Lindsey), and the Hawaii Community Foundation 20080485 (Dr. Jourdan Le Saux).

References

Augustus AS, Buchanan J, Gutman E, Rengo G, Pestell RG, et al. Hearts lacking caveolin-1 develop hypertrophy with normal cardiac substrate metabolism. Cell Cycle. 2008; 7:2509–2518. [PubMed: 18719368]

Barth K, Gentsch M, Blasche R, Pfuller A, Parshyna I, et al. Distribution of caveolin-1 and connexin43 in normal and injured alveolar epithelial R3/1 cells. Histochem Cell Biol. 2005; 123:239–247. [PubMed: 15856276]

Bernatchez PN, Bauer PM, Yu J, Prendergast JS, He P, Sessa WC. Dissecting the molecular control of endothelial NO synthase by caveolin-1 using cell-permeable peptides. Proc Natl Acad Sci U S A. 2005; 102:761–766. [PubMed: 15637154]

Bucci M, Gratton JP, Rudic RD, Acevedo L, Roviezzo F, et al. In vivo delivery of the caveolin-1 scaffolding domain inhibits nitric oxide synthesis and reduces inflammation. Nat Med. 2000; 6:1362–1367. [PubMed: 11100121]

Bujak M, Frangogiannis NG. The role of TGF-beta signaling in myocardial infarction and cardiac remodeling. Cardiovasc Res. 2007; 74:184–195. [PubMed: 17109837]

Bujak M, Ren G, Kweon HJ, Dobaczewski M, Reddy A, et al. Essential role of Smad3 in infarct healing and in the pathogenesis of cardiac remodeling. Circulation. 2007; 116:2127–2138. [PubMed: 17967775]

Chen YG. Endocytic regulation of TGF-beta signaling. Cell Res. 2009; 19:58–70. [PubMed: 19050695]

Chow AK, Cena J, El-Yazbi AF, Crawford BD, Holt A, et al. Caveolin-1 inhibits matrix metalloproteinase-2 activity in the heart. J Mol Cell Cardiol. 2007; 42:896–901. [PubMed: 17349656]

Chow AK, Daniel EE, Schulz R. Cardiac function is not significantly diminished in hearts isolated from young caveolin-1 knockout mice. Am J Physiol Heart Circ Physiol. 299:H1183–1189. [PubMed: 20693397]

Cohen AW, Park DS, Woodman SE, Williams TM, Chandra M, et al. Caveolin-1 null mice develop cardiac hypertrophy with hyperactivation of p42/44 MAP kinase in cardiac fibroblasts. Am J Physiol Cell Physiol. 2003; 284:C457–474. [PubMed: 12388077]

Del Galdo F, Lisanti MP, Jimenez SA. Caveolin-1, transforming growth factor-beta receptor internalization, and the pathogenesis of systemic sclerosis. Curr Opin Rheumatol. 2008; 20:713–719. [PubMed: 18949888]

Duvernelle C, Freund V, Frossard N. Transforming growth factor-beta and its role in asthma. Pulm Pharmacol Ther. 2003; 16:181–196. [PubMed: 12850120]

Farhat N, Thorin-Trescases N, Voghel G, Villeneuve L, Mamarbachi M, et al. Stress-induced senescence predominates in endothelial cells isolated from atherosclerotic chronic smokers. Can J Physiol Pharmacol. 2008; 86:761–769. [PubMed: 19011671]

Galdo FD, Sotgia F, de Almeida CJ, Jasmin JF, Musick M, et al. Decreased expression of caveolin 1 in patients with systemic sclerosis: Crucial role in the pathogenesis of tissue fibrosis. Arthritis Rheum. 2008; 58:2854–2865. [PubMed: 18759267]

Hao J, Ju H, Zhao S, Junaid A, Scammell-La Fleur T, Dixon IM. Elevation of expression of Smads 2, 3, and 4, decorin and TGF-beta in the chronic phase of myocardial infarct scar healing. J Mol Cell Cardiol. 1999; 31:667–678. [PubMed: 10198196]

Jensen JA, Kosek JC, Hunt TK, Goodson WH 3rd, Miller DC. Cardiac cryolesions as an experimental model of myocardial wound healing. Ann Surg. 1987; 206:798–803. [PubMed: 3689016]

Kozera L, White E, Calaghan S. Caveolae act as membrane reserves which limit mechanosensitive I(Cl,swell) channel activation during swelling in the rat ventricular myocyte. PLoS One. 2009; 4:e8312. [PubMed: 20011535]

Langlois S, Cowan KN, Shao Q, Cowan BJ, Laird DW. Caveolin-1 and -2 interact with connexin43 and regulate gap junctional intercellular communication in keratinocytes. Mol Biol Cell. 2008; 19:912–928. [PubMed: 18162583]

Le Saux CJ, Teeters K, Miyasato SK, Hoffmann PR, Bollt O, et al. Down-regulation of caveolin-1, an inhibitor of transforming growth factor-beta signaling, in acute allergen-induced airway remodeling. J Biol Chem. 2008; 283:5760–5768. [PubMed: 18056268]

Lee EK, Lee YS, Han IO, Park SH. Expression of Caveolin-1 reduces cellular responses to TGF-beta1 through down-regulating the expression of TGF-beta type II receptor gene in NIH3T3 fibroblast cells. Biochem Biophys Res Commun. 2007; 359:385–390. [PubMed: 17543885]

Martos R, Baugh J, Ledwidge M, O'Loughlin C, Murphy NF, et al. Diagnosis of heart failure with preserved ejection fraction: improved accuracy with the use of markers of collagen turnover. Eur J Heart Fail. 2009; 11:191–197. [PubMed: 19168518]

Munger JS, Harpel JG, Gleizes PE, Mazzieri R, Nunes I, Rifkin DB. Latent transforming growth factor-beta: structural features and mechanisms of activation. Kidney Int. 1997; 51:1376–1382. [PubMed: 9150447]

Murata T, Lin MI, Huang Y, Yu J, Bauer PM, et al. Reexpression of caveolin-1 in endothelium rescues the vascular, cardiac, and pulmonary defects in global caveolin-1 knockout mice. J Exp Med. 2007; 204:2373–2382. [PubMed: 17893196]

O'Quinn MP, Palatinus JA, Harris BS, Hewett KW, Gourdie RG. A Peptide Mimetic of the Connexin43 Carboxyl Terminus Reduces Gap Junction Remodeling and Induced Arrhythmia Following Ventricular Injury. Circ Res. 2011

Patel HH, Tsutsumi YM, Head BP, Niesman IR, Jennings M, et al. Mechanisms of cardiac protection from ischemia/reperfusion injury: a role for caveolae and caveolin-1. FASEB J. 2007; 21:1565–1574. [PubMed: 17272740]

Radauceanu A, Ducki C, Virion JM, Rossignol P, Mallat Z, et al. Extracellular matrix turnover and inflammatory markers independently predict functional status and outcome in chronic heart failure. J Card Fail. 2008; 14:467–474. [PubMed: 18672194]

Razani B, Zhang XL, Bitzer M, von Gersdorff G, Bottinger EP, Lisanti MP. Caveolin-1 regulates transforming growth factor (TGF)-beta/SMAD signaling through an interaction with the TGF-beta type I receptor. J Biol Chem. 2001; 276:6727–6738. [PubMed: 11102446]

Schubert AL, Schubert W, Spray DC, Lisanti MP. Connexin family members target to lipid raft domains and interact with caveolin-1. Biochemistry. 2002; 41:5754–5764. [PubMed: 11980479]

Tourkina E, Richard M, Gooz P, Bonner M, Pannu J, et al. Antifibrotic properties of caveolin-1 scaffolding domain in vitro and in vivo. Am J Physiol Lung Cell Mol Physiol. 2008; 294:L843–861. [PubMed: 18203815]

van Amerongen MJ, Harmsen MC, van Rooijen N, Petersen AH, van Luyn MJ. Macrophage depletion impairs wound healing and increases left ventricular remodeling after myocardial injury in mice. Am J Pathol. 2007; 170:818–829. [PubMed: 17322368]

van den Bos EJ, Mees BM, de Waard MC, de Crom R, Duncker DJ. A novel model of cryoinjury-induced myocardial infarction in the mouse: a comparison with coronary artery ligation. Am J Physiol Heart Circ Physiol. 2005; 289:H1291–1300. [PubMed: 15863462]

Vanhoutte D, Heymans S. TIMPs and cardiac remodeling: ‘Embracing the MMP-independent-side of the family’. J Mol Cell Cardiol. 2009

Voghel G, Thorin-Trescases N, Farhat N, Nguyen A, Villeneuve L, et al. Cellular senescence in endothelial cells from atherosclerotic patients is accelerated by oxidative stress associated with cardiovascular risk factors. Mech Ageing Dev. 2007; 128:662–671. [PubMed: 18022214]

Volonte D, McTiernan CF, Drab M, Kasper M, Galbiati F. Caveolin-1 and caveolin-3 form heterooligomeric complexes in atrial cardiac myocytes that are required for doxorubicin-induced apoptosis. Am J Physiol Heart Circ Physiol. 2008; 294:H392–401. [PubMed: 17982011]

Wang B, Hao J, Jones SC, Yee MS, Roth JC, Dixon IM. Decreased Smad 7 expression contributes to cardiac fibrosis in the infarcted rat heart. Am J Physiol Heart Circ Physiol. 2002; 282:H1685–1696. [PubMed: 11959632]

Wang B, Omar A, Angelovska T, Drobic V, Rattan SG, et al. Regulation of collagen synthesis by inhibitory Smad7 in cardiac myofibroblasts. Am J Physiol Heart Circ Physiol. 2007; 293:H1282–1290. [PubMed: 17513491]

Wang J, Xu N, Feng X, Hou N, Zhang J, et al. Targeted disruption of Smad4 in cardiomyocytes results in cardiac hypertrophy and heart failure. Circ Res. 2005; 97:821–828. [PubMed: 16151019]

Wang le F, Patel M, Razavi HM, Weicker S, Joseph MG, et al. Role of inducible nitric oxide synthase in pulmonary microvascular protein leak in murine sepsis. Am J Respir Crit Care Med. 2002; 165:1634–1639. [PubMed: 12070065]

Wang XM, Zhang Y, Kim HP, Zhou Z, Feghali-Bostwick CA, et al. Caveolin-1: a critical regulator of lung fibrosis in idiopathic pulmonary fibrosis. J Exp Med. 2006; 203:2895–2906. [PubMed: 17178917]

Williams TM, Medina F, Badano I, Hazan RB, Hutchinson J, et al. Caveolin-1 gene disruption promotes mammary tumorigenesis and dramatically enhances lung metastasis in vivo. Role of Cav-1 in cell invasiveness and matrix metalloproteinase (MMP-2/9) secretion. J Biol Chem. 2004; 279:51630–51646. [PubMed: 15355971]

Young LH, Ikeda Y, Lefer AM. Caveolin-1 peptide exerts cardioprotective effects in myocardial ischemia-reperfusion via nitric oxide mechanism. Am J Physiol Heart Circ Physiol. 2001; 280:H2489–2495. [PubMed: 11356603]

Zhang XL, Topley N, Ito T, Phillips A. Interleukin-6 regulation of transforming growth factor (TGF)-beta receptor compartmentalization and turnover enhances TGF-beta1 signaling. J Biol Chem. 2005; 280:12239–12245. [PubMed: 15661740]

Zhao YY, Liu Y, Stan RV, Fan L, Gu Y, et al. Defects in caveolin-1 cause dilated cardiomyopathy and pulmonary hypertension in knockout mice. Proc Natl Acad Sci U S A. 2002; 99:11375–11380. [PubMed: 12177436]

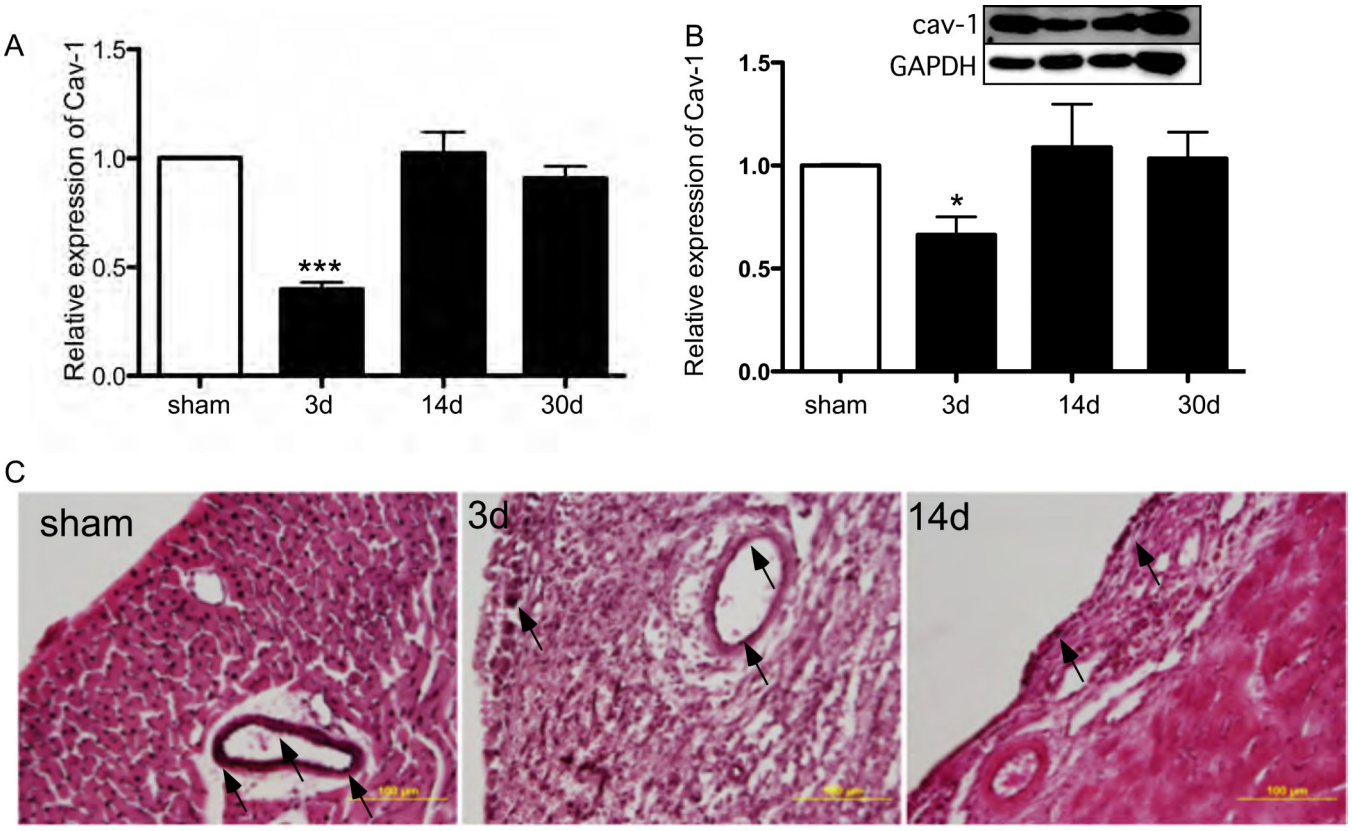

Figure 1. Transiently reduced expression of caveolin-1 in heart following cryoinjury

A) *Cav1* mRNA abundance in cryoinjured WT mice was transiently decreased, compared to sham-operated mice. Gene expression was assessed by TaqMan assay and normalized to ß-actin. WT sham group value has been used for normalization among study groups. Bar represents mean ± SD. ***= $p<0.001$, n= 7. **B)** Measure of level of cav1 protein expression in sham and 3-day post cryoinjured hearts. In insert, a representative western blot from which these data were derived. **C)** Representative immunohistochemistry staining for cav1. This protein is robustly expressed in endothelial cells in sham LV (left), while protein levels dramatically decrease at 3 days after cryoinjury (middle) and are returned towards control at day 14 (right).

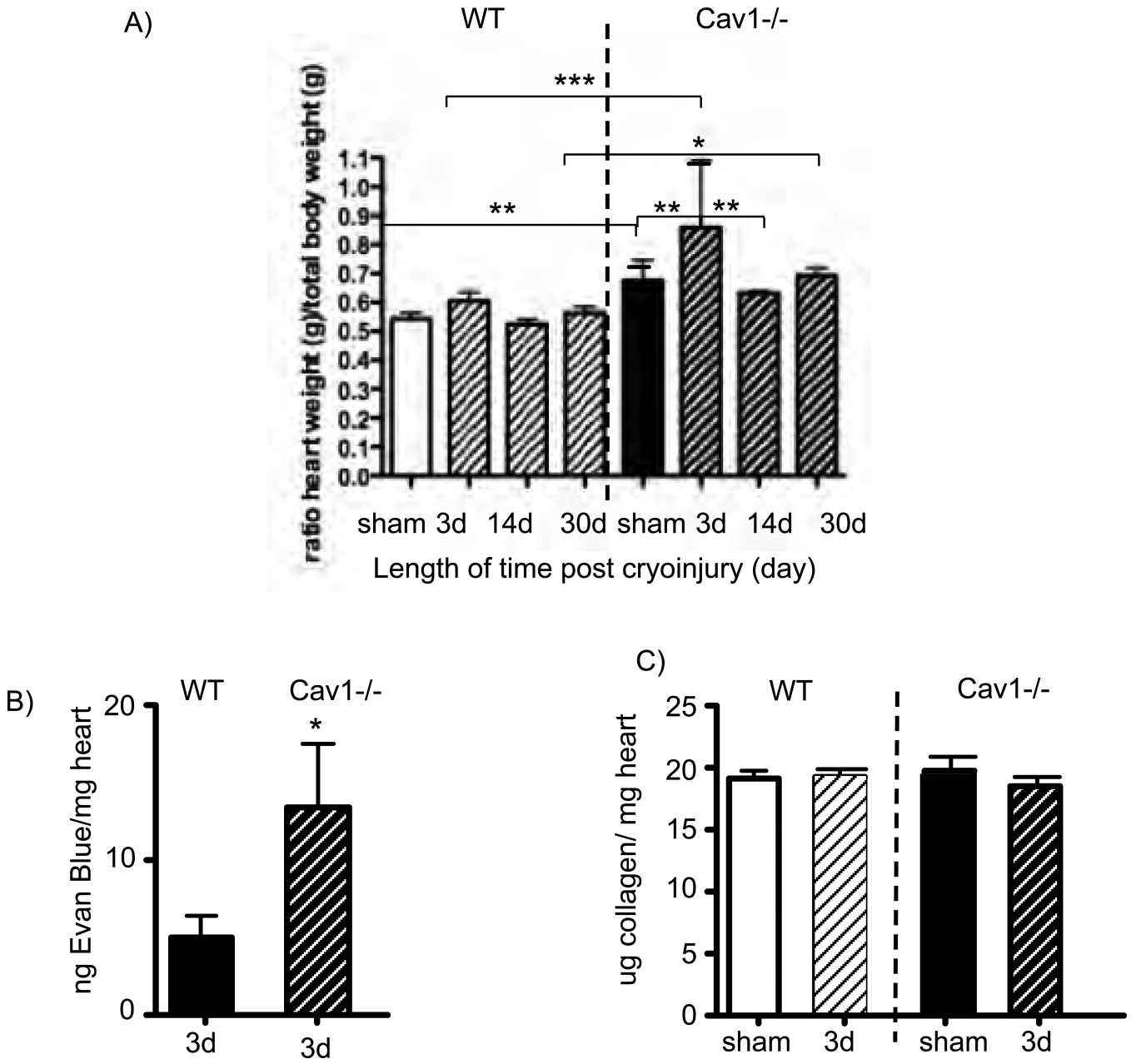

Figure 2. Transient increase in heart weight following cryoinjury in *Cav1*$^{-/-}$ mice

A) Hearts were weighed immediately after the death in sham-operated mice and 3, 14, or 30 days post cryoablation. The bars represent the ratio of total heart weight/total body weight (n≥10 per group). **B)** Quantitative spectrophotometric measurements of Evans Blue dye as a marker of vascular leakage. Three-days after cryoinjury *Cav1*$^{-/-}$ and WT mice were injected with Evans Blue dye. The level of Evans Blue was measured in the heart 24 hr after injection (n = 5 per group). **C)** Total new collagen deposition was evaluated by Sircol as described in the Material and Methods section (n = 5 mice per group). Data are expressed as mean ± standard deviation. *: $p<0.05$; **: $p<0.01$; and ***: $p<0.001$.

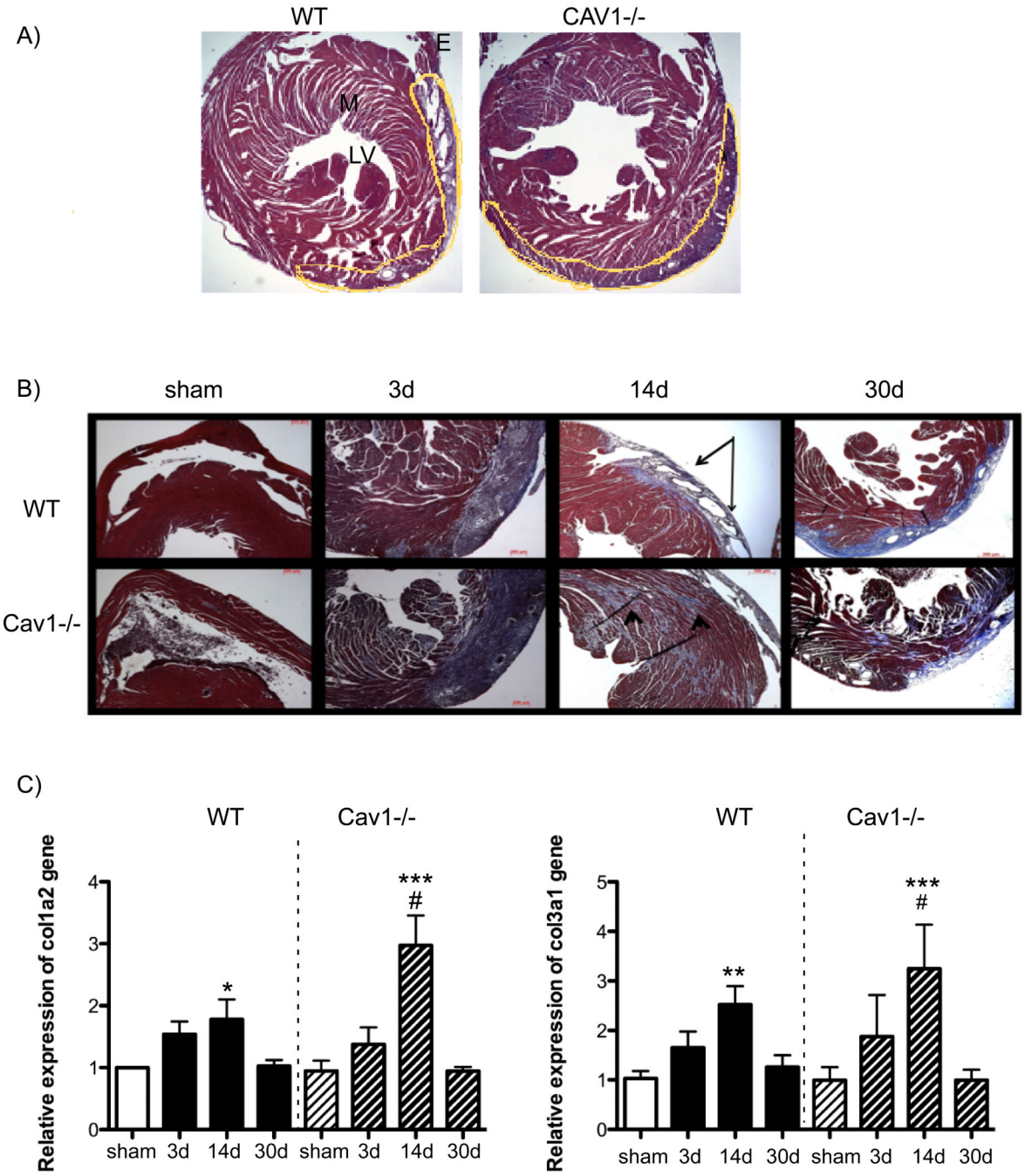

Figure 3. Visualization of the injured border zone and development of cardiac remodeling in cryoinjured heart samples

A) The injured border zone can be visualized by standard HE staining. The injured is outlined by yellow line on the representative sections. E: epicardium; LV: left ventricle; M: myocardium; RV: right ventricle. **B)** Representative photomicrographs of trichrome-stained heart sections from sham-operated and cryoinjured *Cav1*$^{-/-}$ and WT animals; The collagen network is stained in blue and the nuclei of the cells in purple. **C)** The *procol1a2* and *procol3a1* expression in cryoinjured mice increased after 3 days, with an even higher level

at 14 days, and returned to that seen in sham-operated samples by 30 days (n = 7). *: $p<0.05$; **: $p<0.01$; and ***: $p<0.001$.

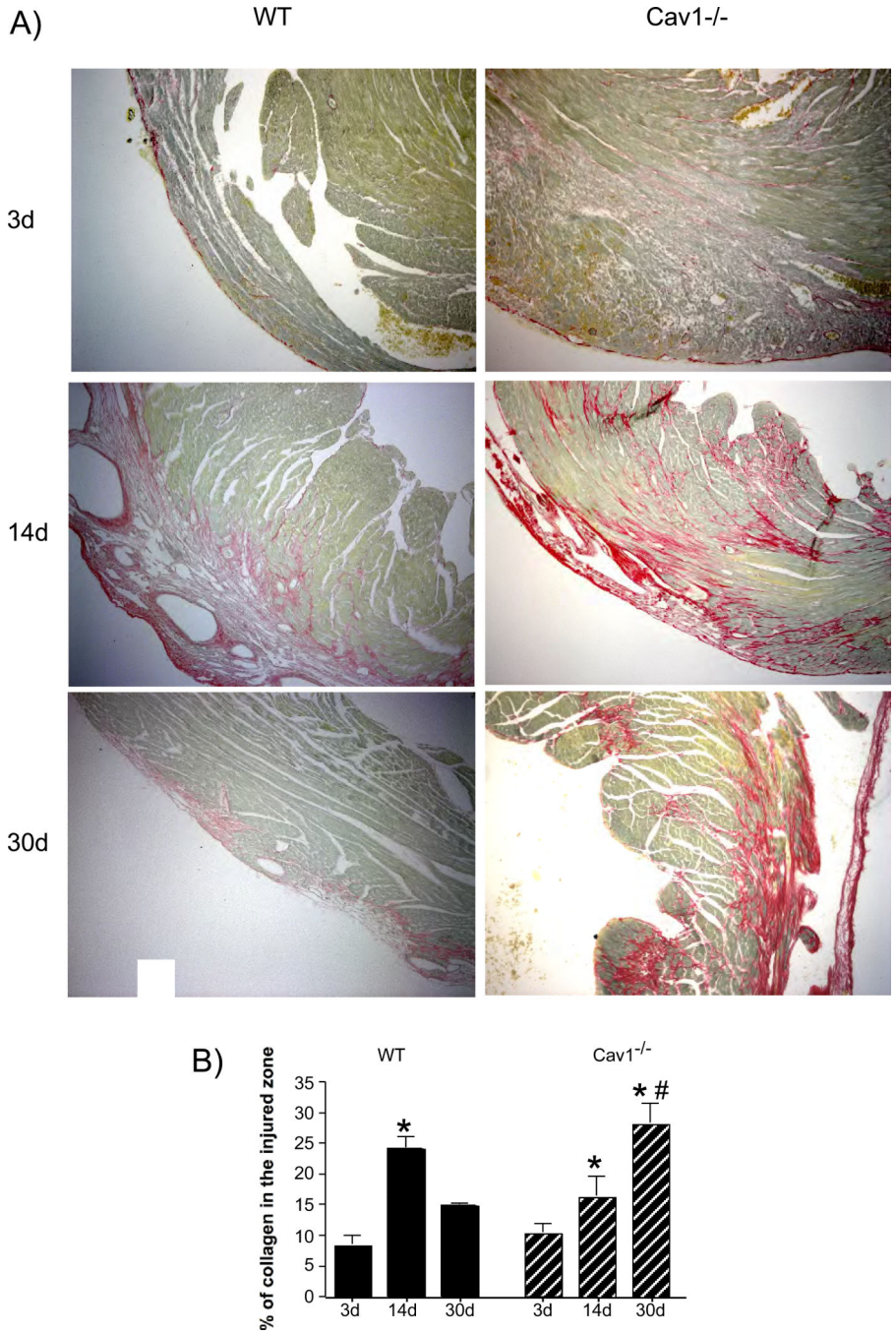

Figure 4. Increased collagen deposition in cryoinjured *Cav1*$^{-/-}$ hearts compared to WT animals

A) Representative photomicrographs of picrosirius red stained heart sections from cryoinjured WT and *Cav1*$^{-/-}$ mice. The collagen network is stained in red. The scar contained a large amount of collagen, which peaked at 14 days post injury in WT. The extent of collagen deposition decreased thereafter. By contrast, *Cav1*$^{-/-}$ mice had increased collagen deposition in the injured region that extended into the non-infarcted myocardium. This accumulation of collagen is still visible after 30 days of injury. **B**) Quantitative analysis demonstrated that *Cav1*$^{-/-}$ mice had significantly more collagen deposition than WT

animals. *: $p<0.05$ (statistical analysis in the same strain) #: $p<0.05$ indicates a statistical difference between WT and *Cav1*$^{-/-}$ at the same time point.

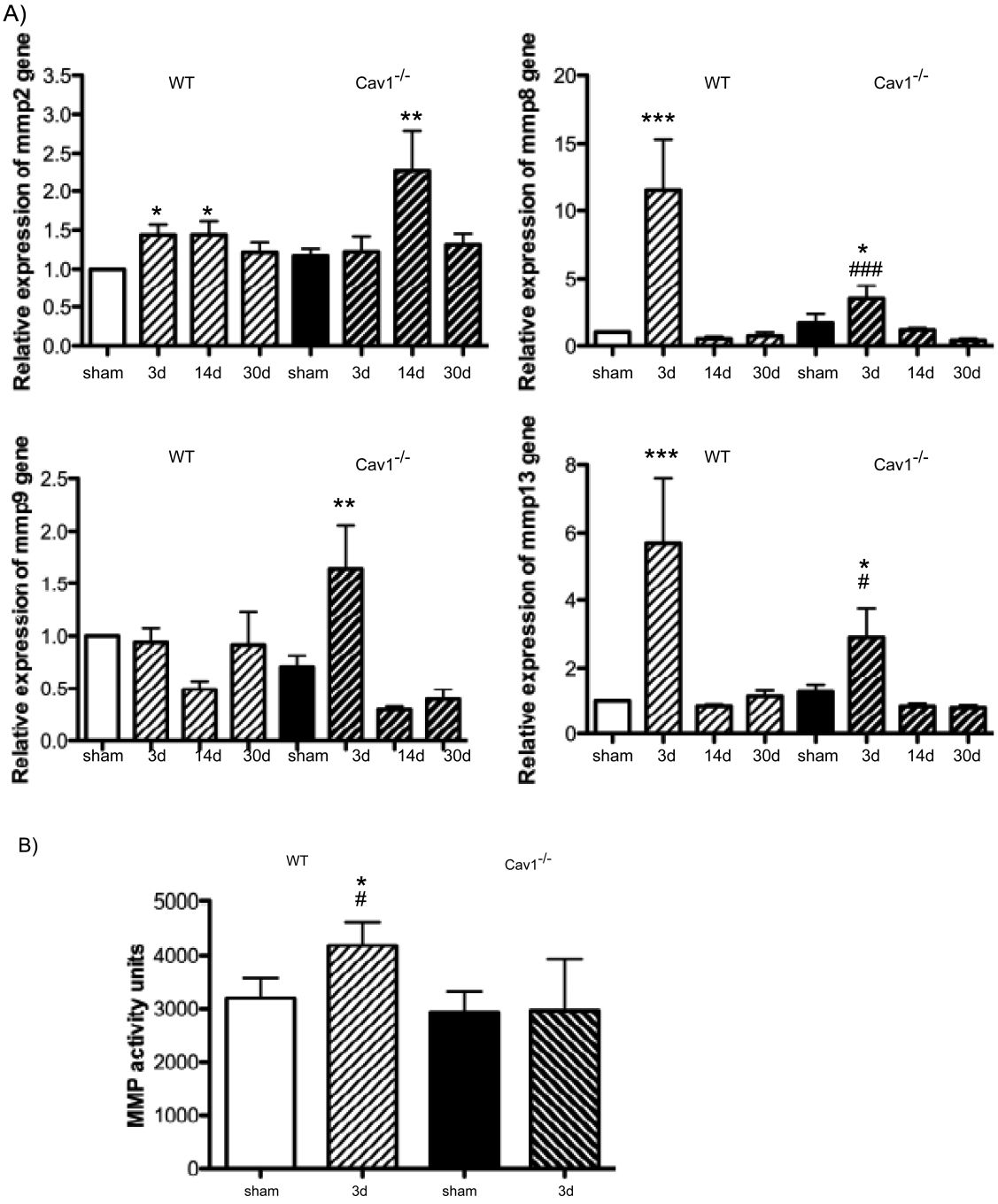

Figure 5. Altered MMP activation in Cav1−/− mice after cryoinjury

A) MMP-2, −8, −9 and −13 mRNA abundance in WT and *Cav1*$^{-/-}$ heart after cryoablation. The level of *MMP* expression was determined in *Cav1*$^{-/-}$ and WT mice by qPCR with TaqMan probes specific to the murine cDNA −3d, −14d, or −30d post injury and compared to sham. The results were normalized to the GAPDH expression. The assays were performed in triplicate. **B)** Total MMP activity was measured. Data are expressed as mean ± SD. *: $p<0.05$; **: $p<0.01$; ***: $p<0.001$ (statistical analysis in the same strain) #: $p<0.05$; ##:

p<0.01; ###: p<0.001 indicates a statistical difference between WT and *Cav1*$^{-/-}$ at the same time point.

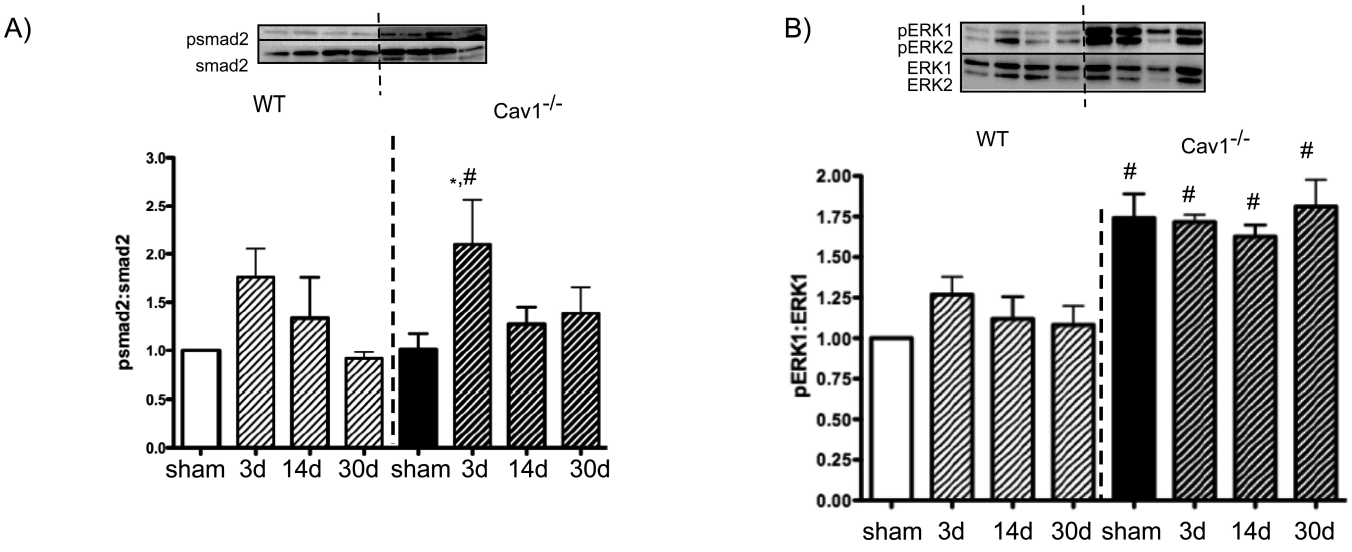

Figure 6.

Activation of TGF-β signaling following cryoinjury was assessed by measuring phosphorylation of Smad2 and ERK1 in mouse heart following cryoablation. Bar represents mean ± SD. **= $p<0.01$ between 2 time points for the same strain; # = $p<0.05$ and ## = $p<0.01$ between both strains for the same time point, n= 5-10.

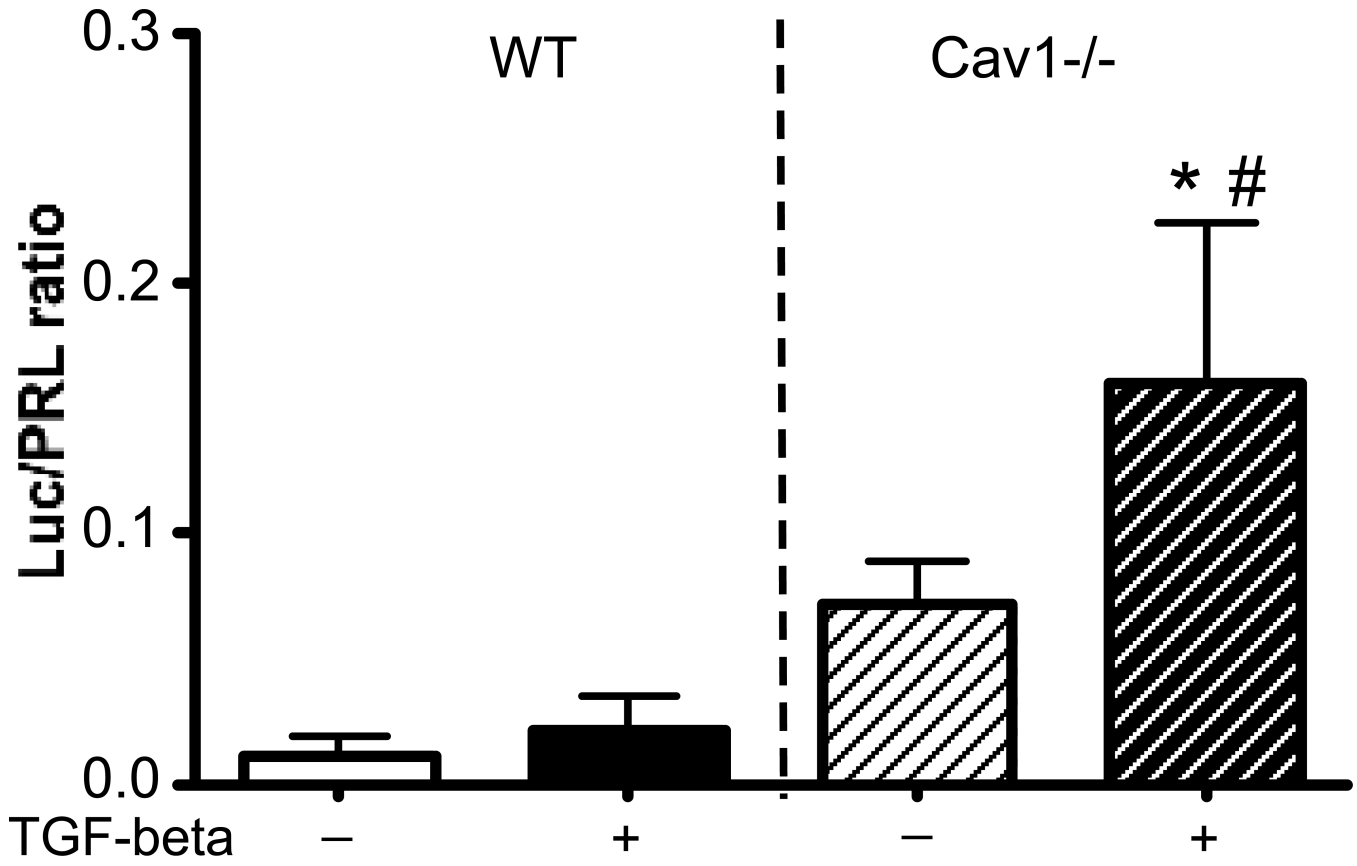

Figure 7. Enhanced activity of TGF-β1 signaling in TGF–β1-stimulated lung fibroblasts lacking cav1 expression

The Smad response element construct was transfected into heart fibroblasts extracted from WT and *Cav1*$^{-/-}$. These fibroblasts were transfected with 1μg of plasmid and 0.1 μg of pRL-SV40 plasmid for control purposes and cultured for 24 hr with 2 ng/ml of TGF-β1. *Luciferase* activity was normalized to the *renilla luciferase* activity. Each value represents the mean ± SD of at least three independent transfection experiments, each performed in triplicate. *: $p<0.05$; and **: $p<0.01$ (statistical analysis in the same strain) #: $p<0.05$ indicates a statistical difference between WT and *Cav1*$^{-/-}$ at the same time point.

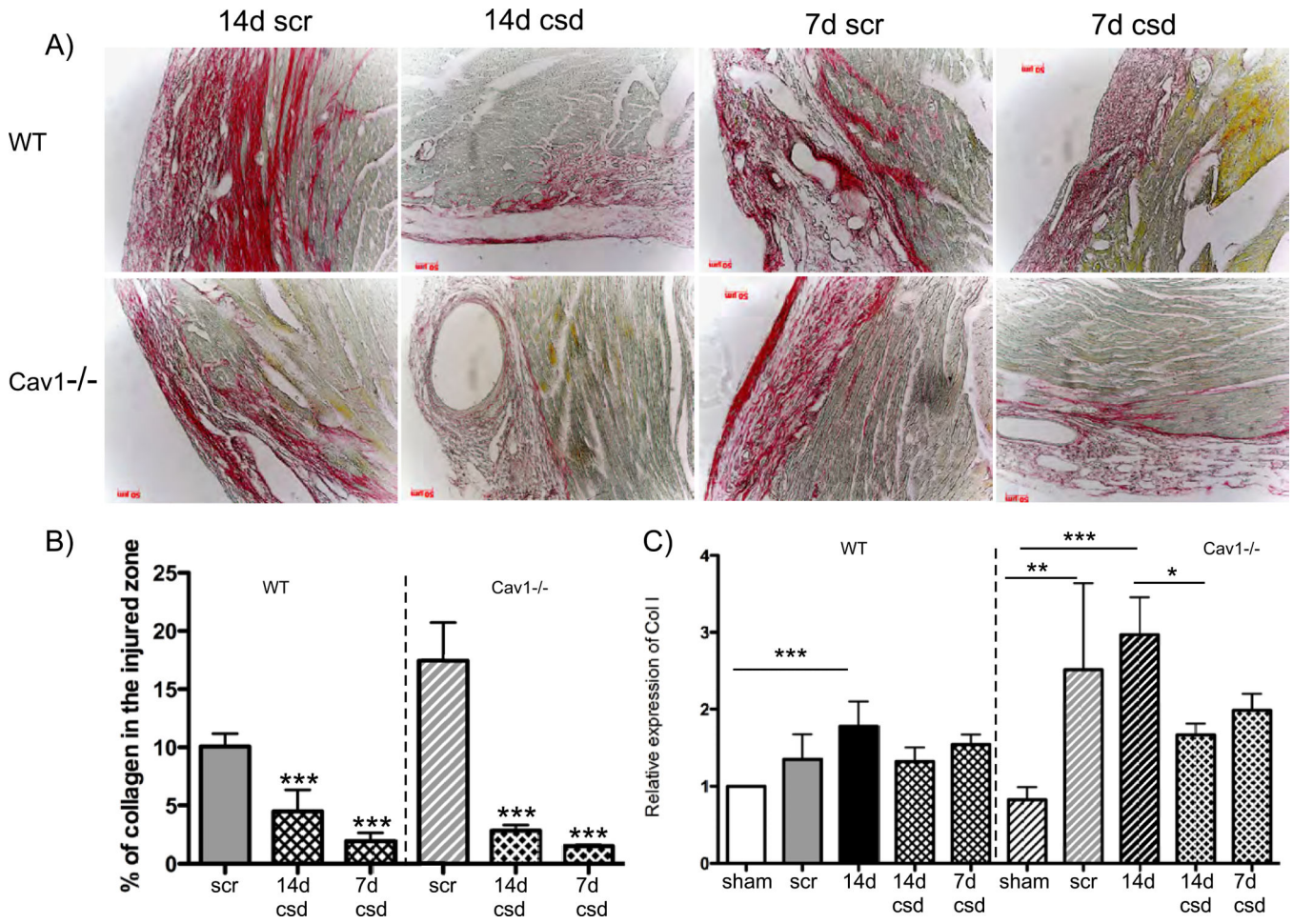

Figure 8. Cav1 scaffolding domain (CSD) peptide treatment prevents increased collagen deposition in cryoinjured myocardium

Representative photomicrographs of picrosirius red stained heart sections from cryoinjured WT and *Cav1*$^{-/-}$ mice. The collagen network is stained in red. The scar contained a large amount of collagen at 14 days post injury when the mice were treated with the scrambled peptide. There is less collagen deposition in the hearts of mice treated with the CSD peptide for both strains. **B)** Qualitative analysis of picrosirius red stained heart sections demonstrated that *Cav1*$^{-/-}$ mice had significantly more collagen deposition than WT animals at 14 days when treated with the scrambled peptide. Administration of the CSD peptide prevented the accumulation of collagen. **C)** The *procol1a2* expression in cryoinjured mice treated with CSD was reduced in both *Cav1*$^{-/-}$ and WT mice.

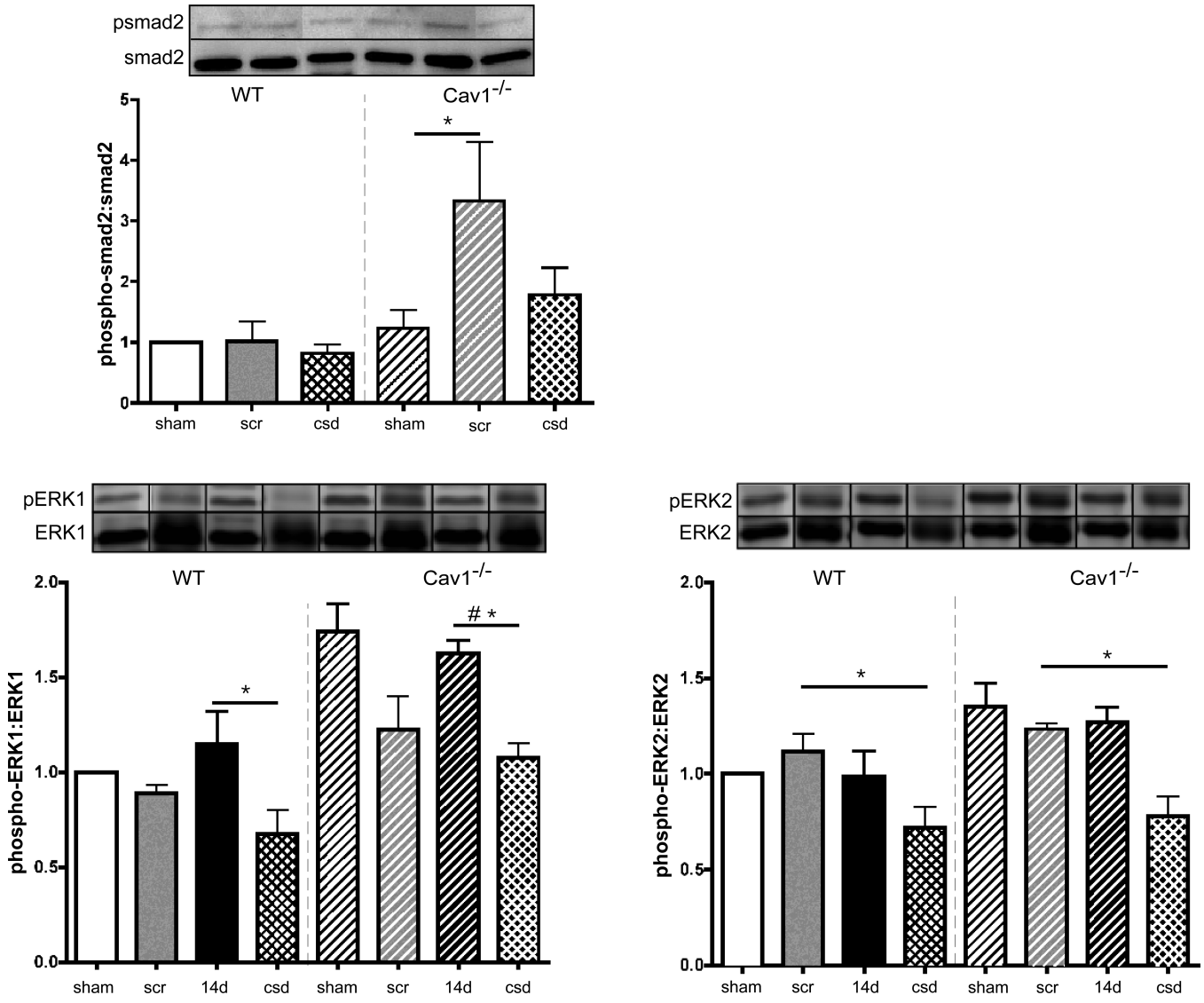

Figure 9. Representative Western Blot analysis of Smad2, pSmad2, ERK1/2, and pERK1/2 in WT and *Cav1*$^{-/-}$ heart samples treated with the Cav1 scaffolding domain (CSD) peptide

Bar represents the mean of the ratio of phosphorylated/total signaling proteins. Values are represented as mean ± SD. **: $p<0.01$; and ***: $p<0.001$ (statistical analysis in the same strain) #: $p<0.05$ indicates a statistical difference between WT and *Cav1*$^{-/-}$ at the same time point. Scr: scrambled peptide and CSD: caveolin 1 scaffolding domain

Table 1

Inflammatory responses after cryoinjury.

		WT				Cav1−/−			
		sham	**3d**	**14d**	**30d**	**sham**	**3d**	**14d**	**30d**
Infiltrating cell	Neutrophil (cells/625μm^2)	1.38 ± 0.23	54.3 ± 11.4	1.00 ± 0.25	3.03 ± 0.68	1.05 ± 0.20	59.9 ± 2.5	0.850 ± 0.187	2.35 ± 0.38
	Macrophage (cells/625μm^2)	4.43 ± 1.89	111 ± 16	64.1 ± 29.0	9.76 ± 3.36	1.32 ± 0.40	98.4 ± 26.7	6.75 ± 3.84	4.10 ± 1.82
Cytokine	IL-1β	1	2.38 ± 0.24	0.962 ± 0.202	1.59 ± 0.37	1.52 ± 0.45	1.93 ± 0.48	1.32 ± 0.12	0.869 ± 0.164
	IL-6	1	6.38 ±1.23	0.825 ± 0.207	2.85 ± 21	2.39 ± 0.74	11.8 ± 3.5	3.47 ± 0.33	1.95 ± 0.17
	TNF-α	1	2.79 ± 0.74	2.92 ± 0.35	1.15 ± 0.23	2.38 ± 0.92	2.17 ± 0.51	1.74 ± 0.15	1.21 ± 0.28
	TGF-β	1	0.712 ± 0.012	1.267 ± 0.07	1.27 ± 0.07	1.24 ± 0.10	1.06 ± 0.10	2.14 ± 0.33	1.38 ± 0.12

Upper part:Neutrophils and macrophages were identified by immunohistochemistry in injured WT and *Cav1*$^{-/-}$ knockout (Cav1−/−) hearts after 3 days, 14 days, and 30 days after cryoinjury. **Lower part:** Expression of proinflammatory cytokines in the whole heart of WT and *Cav1*$^{-/-}$ knockout after 3 days, 14 days, and 30 days after cryoinjury.